Characterisation of bursts in a turbulent boundary layer over circular cavities

Francesco Scarano, Marc Jacob, Xavier Carbonneau, Erwin Ricky Gowree

Association Aéronautique et Astronautique de France

56th 3AF International Conference on Applied Aerodynamics
28 — 30 March 2022, Toulouse – France

FP87-2022-scarano

Characterisation of bursts in a turbulent boundary layer over circular cavities

Francesco Scarano[(1)], Marc C. Jacob[(2)], Xavier Carbonneau[(1)] and Erwin R. Gowree[(1)]
[(1)]*ISAE-SUPAERO, Universite de Toulouse, 10 avenue Edouard Belin, 31055 Toulouse*
[(2)]*Lab. de Mécanique des Fluides et d'Acoustique, UMR 5509 CNRS, Université de Lyon*
Ecole Centrale de Lyon, INSA Lyon, Université Claude Bernard Lyon I,
francesco.scarano@isae-supaero.fr

April 27, 2022

ABSTRACT

Boundary layer surveys are performed to characterise the turbulent boundary layer grazing over a a surface with flush-mounted circular cavities disposed in a staggered arrangement (staggered angle of 45 deg). The momentum thickness based Reynolds number varies from $Re_\theta = 1830$ to 3380 and the cavity diameter and spacing in wall units from $d^+ = 130$ to 250 and $L^+ = 587$ to 1075 respectively. A decrease in the local skin friction drag with respect to a smooth baseline is evidenced as well as a thickening of the viscous sublayer. The bursts frequency profile for the perforated case is shifted away from the wall while the intensity of the bursts is reduced. The production term of the turbulent kinetic energy budget is obtained from Particle Image Velocimetry data. An upward shift and a decrease in magnitude of the peak associated to the streaks suggests that the cavities modify the near wall turbulent cycle.

1. INTRODUCTION

Skin friction drag accounts for more than (50%) of the overall drag for an aircraft in cruise condition. Reducing the skin friction drag would then have a strong impact on the CO_2 emissions reductions since 1% of drag reduction is converted into a 0.75% in fuel-burn savings [11, 8]. The skin friction drag is generated by the turbulent boundary layer grazing over the surfaces of the aircraft. In a turbulent boundary layer the effect of the coherent structures, namely the hairpin vortices largely documented in literature [1], is responsible for the majority of the turbulent kinetic production and transport in the near wall region and the skin friction drag. In particular, the turbulent activity, sometimes called bursting, can be decoupled in sweep ($u > 0$, $v < 0$) and ejections ($u < 0$, $v > 0$) which give a positive contribution to the Reynolds shear stress and to the production of turbulent kinetic energy. The control of this near-wall activity would lead to a potential skin friction reduction [8].

Several techniques have been proposed for skin friction drag reduction; the most studied are the riblets [15, 4] and the spanwise wall oscillations [11, 5, 10]. Despite the different mechanism involved (the riblets inhibit the spanwise movement of the structures while the spanwise wall oscillations impose a spanwise movement) and the charateristic size in wall units (15-20 viscous lengths for the riblets sizes and up to 8000 viscous lengths for the spanwise wall oscillations wavelengths) these techniques have proven to be highly effective in turbulent skin friction drag reduction. Difficulties in the implementations of these techniques lay in the sophisticated manufacturing for the riblets and in the high complexity realisation of spanwise wall oscillations in real life conditions as well as in laboratories [2, 9].

More recently, studies on large dimples [14]) (diameters up to four times the boundary layer thickness) and small cavities [7, 12] (diameter in wall units $20 < d^+ < 145$) have boosted the interest in the application of these wall patterns to reduce the turbulent activity and the skin friction.

The aim of this study is to further investigate the modification of the turbulent activity of a turbulent boundary layer grazing over a staggered array of flush-mounted cavities. This is done by the combination of hot wire surveys and stereoscopic PIV. The diameter and depth of the cavities have been chosen in agreement with the previous studies [7, 12].

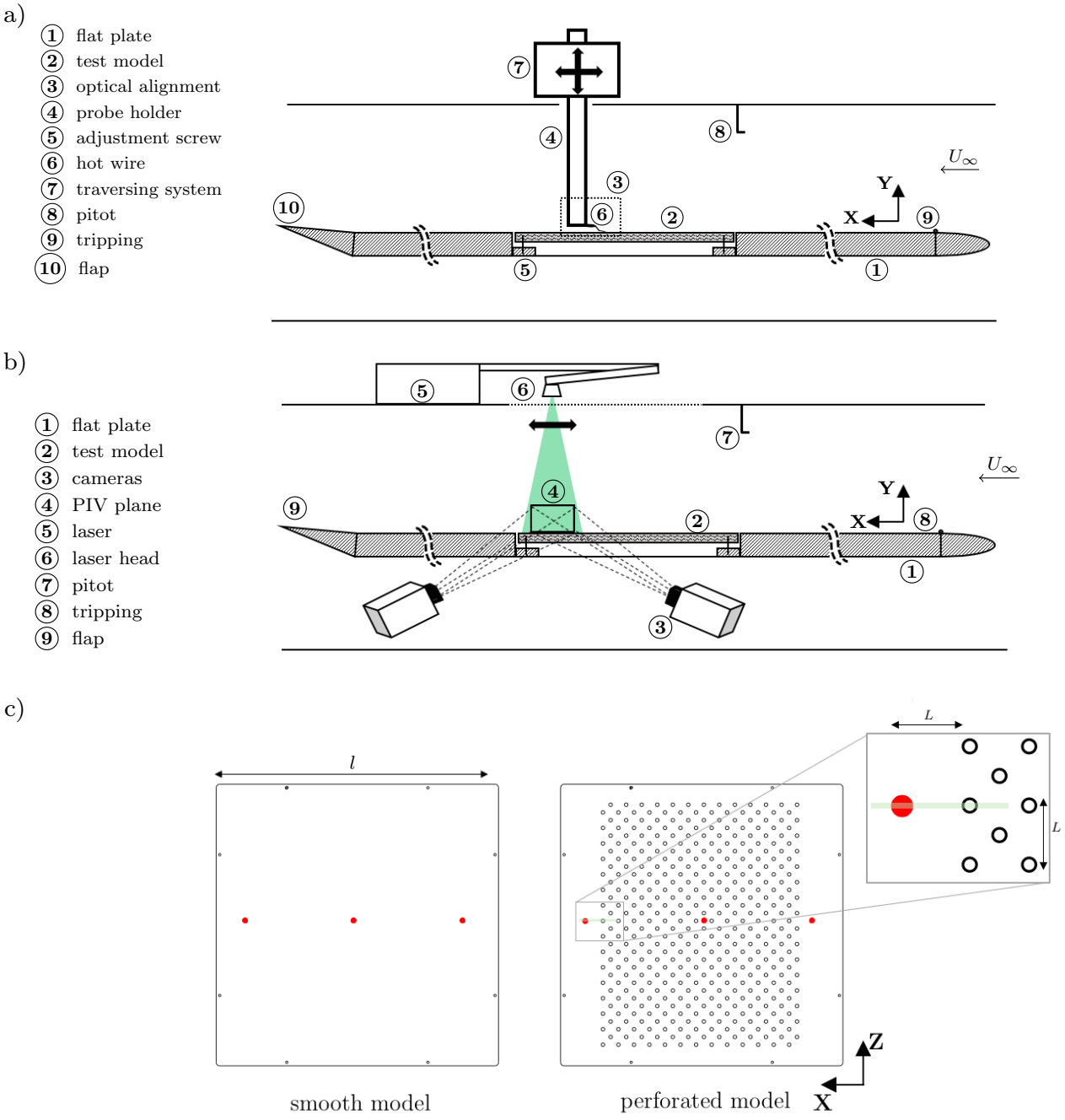

Figure 1: Hot wire setup a), PIV setup b), test models and measurement locations c) (red dots for hot wire measurements, green line for the trace of the PIV plane).

2. METHODS

2.1 Hot wire setup

The experimental campaign has been conducted in the SaBRe wind tunnel at ISAE-SUPAERO. The length of the test section is 2.5 m in the streamwise direction (X), its width is 1.2 m in the horizontal (spanwise) direction (Z), whereas its height is 0.8 m (Y). Inside the test section, a 2.5 m long, 1.2 m wide flat plate was mounted horizontally; the plate has an elliptic leading edge and it is equipped with a flap at the trailing edge. The flap was set at an angle of 3.7° during the entire experimental campaign in order to ensure a zero streamwise pressure gradient along the measurement domain. A Dantec P5517 hot wire probe for boundary layer connected to a two axes traversing system coupled with an optical probe to wall

CASE	U_∞ [m/s]	Re_θ	d^+	h^+	Re_τ	L^+	δ/d	δ/h	u_{τ_0}
a)	10	1830	130	104	580	587	4.3	3.4	0.42
b)	15	2710	190	152	745	838	3.9	3.1	0.60
c)	20	3380	250	200	950	1075	3.7	3.0	0.77

Table 1: Flow and geometrical parameters for the three different test conditions, downstream measurement location.

alignment technique proved to be a reliable method for measurements close to the wall.

2.2 PIV setup

Stereoscopic PIV was used in the current setup. The measurement was in the direction of the flow (XY) at the trailing edge of the cavities. A commercial PIV system from Dantec Dynamics is used for the measurements. The laser is placed on top of the test section and it is connected to a laser arm which allows a precise movement and alignment of the laser sheet along the domain. The laser sheet is shone from the top and passes through a glass ceiling of the wind tunnel. The thickness of the laser sheet is approximately 0.5 mm. To avoid reflections on the models, the bottom part (which is transparent because of the transparent plexiglass) is covered by a black matte film. Black velcro was applied to the surfaces of the tunnel to avoid reflections during the acquisition process. The flow is seeded with a TOPAS smoke generator located downstream of the divergence of the tunnel. Before acquiring each measurements. The seeding system was activated for some time prior to the measurement in order to ensure that the boundary layer was sufficiently seeded.

The images are taken from the sides through the glass wall by two CCD cameras disposed in a steroscopic arrangement equipped with a NIKON 300 mm f/4 lens. DANTEC dynamic studio 6.1 was used for the calibration, for synchronising image acquisition to the laser, and for the calculation of the PIV vectors. The field of view (FOV) is 8.5 mm$\times$4.5 mm. 1000 image pairs are acquired at 50 Hz. The two laser pulses have a Δt which depends on the freesetream velocity and the measurement location, and it was such that a maximum particle displacement in a range of 10 pixels is obtained. For the streamwise planes the Δt used are 15 μs for 10 m/s, 20 μs for 15 m/s and 30 μs for 20 m/s.

The image pairs are processed using the 2D3C cross-correlation PIV algorithm of Dantec Dynamics studio. The interrogation window size is iteratvely changed passing from 32×32 pixel to 16×16 with an overlap of 50%. This leads to a grid of 40400 vectors with a spatial resolution of 0.21 mm ($\Delta X^+, \Delta Y^+ = 4$). Vectors close to the wall Y^+ are discarded due to the reflections at the wall.

2.3 Models and measurements locations

The test samples consist of two square Plexiglas plates of 400 mm by 400 mm and 4 mm thickness, one completely smooth and the other with a staggered array of circular cavities sealed at the bottom. The diameter d of the cavities is 5 mm. The spacing between two cavities on a same row is L =22 mm (4.4d), with a stagger angle of 45°. The characteristic dimensions of the cavities and the three flow conditions are reported in **Table 1**. The hot wire measurements have been performed in the mid-span plane of the model, upstream of the cavities at the middle and downstream of the cavities where the PIV plane has been acquired. The measurement at the leading edge and at trailing edge are at one cavity distance L upstream/downstream of the last row of cavities.

3. RESULTS AND DISCUSSIONS

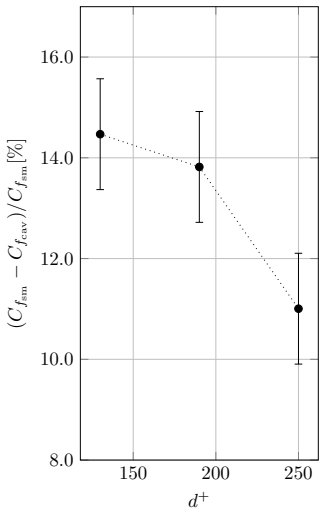

Figure 2: Percentage skin friction reduction obtained using the Clauser chart technique.

In **Fig 3** the mean and RMS velocity profiles downstream the last row of cavities are compared with the corresponding smooth results. The values are reported in wall units and they are obtained using the actual value of the friction velocity calculated using the Clauser chart technique [16]. For the sake of brevity only the results for the 10 m/s case (namely $d^+ = 130$) are reported in **Fig 3**.

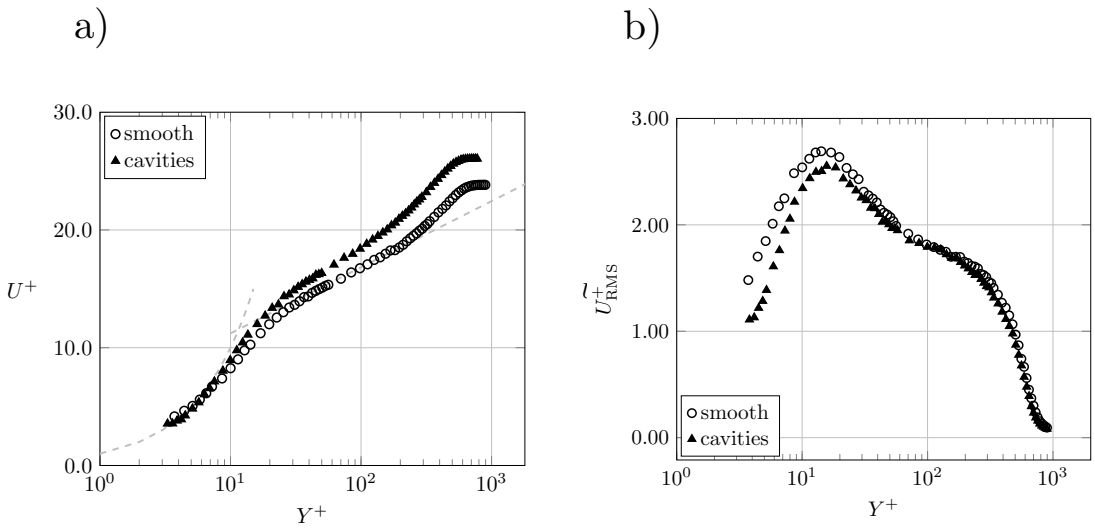

Figure 3: Mean velocity and root mean square of the streamwise velocity in wall units at the trailing edge of the model, $d^+ = 130$.

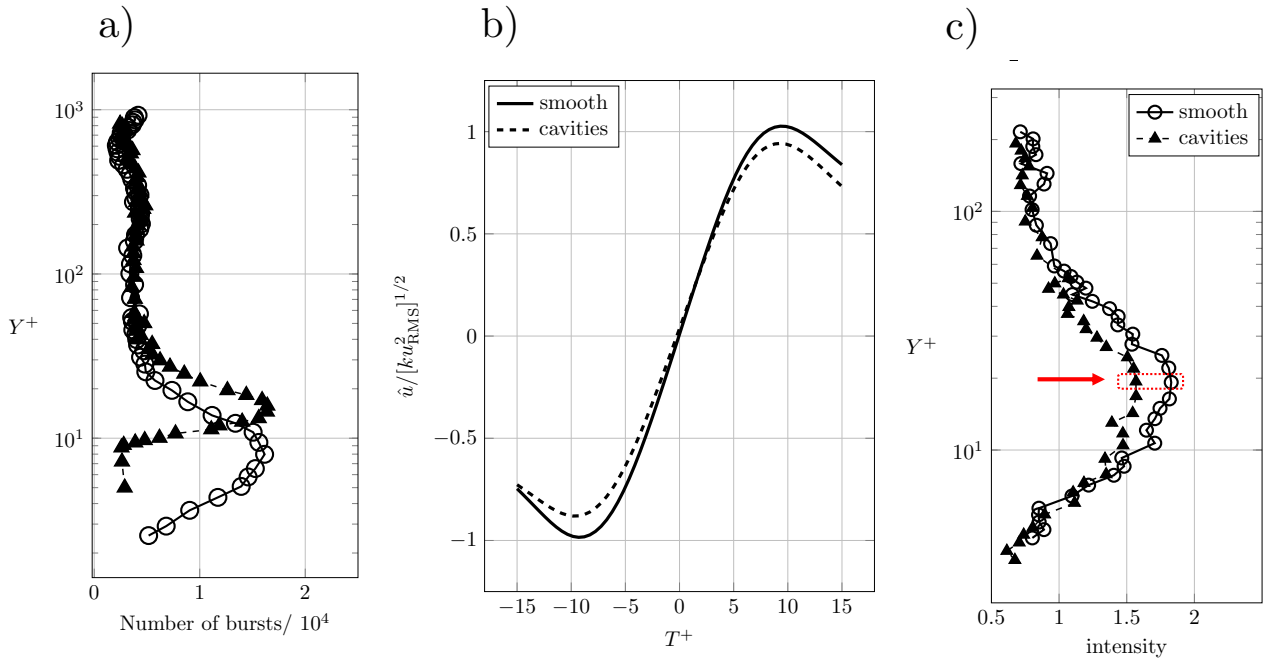

Figure 4: Number of bursts profile a), average burst signature for smooth and perforated b), average burst intensity profile for smooth and perforated c), results for $d^+ = 130$.

A thickening of the viscous sublayer can be evidenced as well as a decrease in the peak of the RMS of the streamwise velocity. These results are in agreement with [7] and [12] and suggest a local skin friction reduction. In **Fig 2** the local skin friction reduction percentage between the perforated and the baseline surface is reported. A local skin friction reduction can be observed for all the freestream conditions but a decrease of the skin friction reduction with d^+ can be evidenced; similar trend are reported in the studies by [7] and [12].

To better understand the turbulent behaviour, the Variable Interval Time Averaging (VITA) technique has been applied to the profiles [3]. This technique, largely used for turbulent boundary layer research, is a simple and powerful way to detect bursts in a turbulent boundary layer. It consists in comparing the short-term RMS to the long-time RMS of the entire signal. If the short-term RMS is larger than the long-term RMS multiplied by a

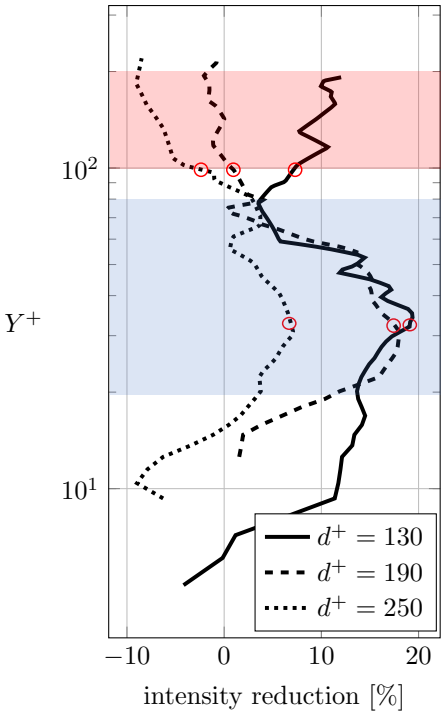

Figure 5: Intensity reduction profile for the three flow conditions.

constant k [13] a burst is detected. The short-term RMS is computed considering a time window which has to be of the order of magnitude of the characteristic time of the passage of a structure $T^+ \cong 15$.

Given a fluctuating quantity $Q(x_i,t)$ the short term average of the variable in the interval time T can be defined as

$$\widehat{Q}(x_i,t,T) = \int_{t-\frac{T}{2}}^{t+\frac{T}{2}} Q(x_i,s)ds \qquad (1)$$

and the short term variance is

$$\widehat{\mathrm{var}}(x_i,t,T) = \widehat{U^2}(x_i,t,T) - [\widehat{U}(x_i,t,T)]^2. \qquad (2)$$

The detection is then based on a Heaviside function

$$D(t) = 1 \quad \text{if} \quad \widehat{\mathrm{var}}(x_i,t,T) > k \cdot U^2_{\mathrm{RMS}}; \quad 0 \quad \text{otherwise} \qquad (3)$$

The VITA technique allow to detect, for each location of the boundary layer, namely for each Y^+, the number of burst and to compute the average burst intensity. This leads to a profile of the bursts frequency and intensity.

In **Fig 4** the results for the $d^+ = 130$ and the comparison with the smooth baseline are presented (similar consideration can be made for the other flow conditions). In **Fig 4** a) one can see that the burst frequency profile for the perforated case is shifted upward by $\Delta Y^+ = 5$. A similar shift has been documented previously for spanwise wall oscillations [5, 6] and riblets [4]. This is in line with the thickening of the boundary layer and suggest an upward shift of the turbulent activity.

When looking at the burst intensity profile, **Fig 4** b), a decrease in the average intensity with respect to the smooth baseline can be observed. This is very clear in the region which corresponds to the lobe at $20 < Y^+ < 80$.

The percentage intensity decrease with respect to the smooth baseline is reported in **Fig 5** for the three flow conditions. As for the friction coefficient, the intensity reduction is more pronounced for the lower d^+ and decreases when increasing the d^+ namely the Reynolds number. This results is in agreement with what found by Silvestri et al. [12] who applied the technique only for $Y^+ = 100$ (see red dots in **Fig 5**). Their study highlighted the loss of benefit in terms of intensity reduction for values of d^+ above 145. On contrary, the results reported in **Fig 5** show that even for higher values of d^+ (190 and 250) there is an entire region of the boundary layer ($20 < Y^+ < 80$ highlighted in blue) where the intensity reduction is positive. These results are in agreement with the local skin friction measurements reported in **Fig 2**.

In **Fig 6** a) a snapshot of the streamwise velocity contour is reported, again only for $d^+ = 130$. In the region downstream of the last row of cavities, the turbulent kinetic energy production term is evaluated

$$P = \overline{uv}\frac{d\overline{U}}{dY}. \qquad (4)$$

The production term is averaged in the region downstream of the cavity and the average profile is reported in **Fig 6** b). An upward shift and an attenuation of the first peak of the turbulent kinetic energy production term has to be highlighted. The first peak is associated with the near wall cycle and the kinetic energy produced by the streaks close to the wall. Interestingly, the second peak which is associated with the shear layer of the boundary layer is increased in magnitude suggesting an overall upward shift of the turbulent kinetic energy production. These results are in agreement with the VITA results presented in **Fig 4**.

Quadrant Analysis in the downstream region (results not reported here) revealed that the attenuation of the inner peak is due to an attenuation of the sweeps closer to the wall. Conversely the ejections increases in the logarithmic layer justifying the increase of the outer peak.

4. CONCLUSION & FURTHER WORKS

Turbulent boundary layer measurements have been conducted on a surface with flush-mounted circular cavities disposed in a staggered arrangement. The measurements have been conducted by means of hot wire surveys and stereoscopic PIV at three different flow conditions resulting in d^+ between 130 and 250. The cavities modify the near wall turbulent cycle, shifting upwardly and attenuating the production term of the turbulent kinetic energy

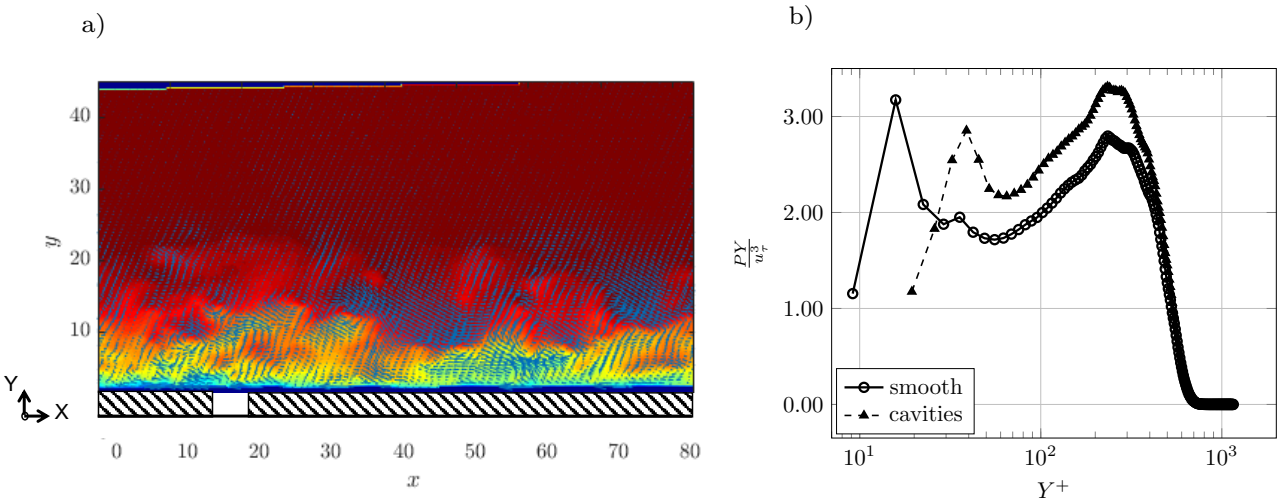

Figure 6: Contour of a snapshot of the streamwise velocity field a), average turbulent kinetic energy production term b).

budget. This is due to an overall attenuation of burst intensity in the region $20 < Y^+ 80$ and an upward shift of the burst frequency. The modification of the turbulence is translated into a thickening of the viscous sublayer and a local skin friction reduction. Further works are encouraged to

1. verify the spanwise uniformity of the aforementioned behaviour

2. study separately the effect of geometrical parameters (d^+, L^+) and the flow condition.

5. ACKNOWLEDGEMENTS

The authors thank the AID (Agence Innovation Défense) for their financial support to the FriDA project.

REFERENCES

[1] Ronald J. Adrian. Hairpin vortex organization in wall turbulence. *Physics of Fluids*, 19(4):041301, 2007.

[2] F. Auteri, A. Baron, M. Belan, G. Campanardi, and M. Quadrio. Experimental assessment of drag reduction by traveling waves in a turbulent pipe flow. *Physics of Fluids*, 22(11):115103, 2010.

[3] R. F. Blackwelder and R. E. Kaplan. On the wall structure of the turbulent boundary layer. *Journal of Fluid Mechanics*, 76(1):89–112, 1976.

[4] K.S. Choi. Near-wall structure of a turbulent boundary layer with riblets. *Journal of Fluid Mechanics*, 208:417–458, 11 1989.

[5] Kwing-So Choi, Jean-Robert DeBisschop, and Brian R. Clayton. Turbulent boundary-layer control by means of spanwise-wall oscillation. *AIAA Journal*, 36(7):1157–1163, 1998.

[6] Gaetano Maria Di Cicca, Gaetano Iuso, Pier Giorgio Spazzini, and Michele Onorato. Particle image velocimetry investigation of a turbulent boundary layer manipulated by spanwise wall oscillations. *Journal of Fluid Mechanics*, 467:41–56, 2002.

[7] E.R. Gowree, C. Jagadeesh, and C.J. Atkin. Skin friction drag reduction over staggered three dimensional cavities. *Aerospace Science and Technology*, 84:520–529, 2019.

[8] Michael A. Leschziner. Friction-drag reduction by transverse wall motion – a review. *Journal of Mechanics*, 36(5):649–663, 2020.

[9] Ivan Marusic, Dileep Chandran, Amirreza Rouhi, Matt fu, David Wine, Brian Holloway, Daniel Chung, and Alexander Smits. An energy-efficient pathway to turbulent drag reduction. *Nature Communications*, 12, 10 2021.

[10] Maurizio Quadrio, Pierre Ricco, and Claudio Viotti. Streamwise-travelling waves of spanwise wall velocity for turbulent drag reduction. *Journal of Fluid Mechanics*, 627:161–178, 2009.

[11] Pierre Ricco, Martin Skote, and Michael A Leschziner. A review of turbulent skin-friction drag reduction by near-wall transverse forcing. *Progress in Aerospace Sciences*, 123, 2021.

[12] Anton Silvestri, Farzin Ghanadi, Maziar Arjomandi, Ben Cazzolato, and Anthony Zander. Attenuation of sweep events in a turbulent boundary

layer using micro-cavities. *Experiments in Fluids*, 58, 04 2017.

[13] P Sullivan and A Pollard. Coherent structure identification from the analysis of hot-wire data. *Measurement Science and Technology*, 7(10):1498–1516, oct 1996.

[14] M. van Nesselrooij, L. L. M. Veldhuis, B. W. van Oudheusden, and F. F. J. Schrijer. Drag reduction by means of dimpled surfaces in turbulent boundary layers. *Experiments in Fluids*, 57(9):142, Aug 2016.

[15] M. J. Walsh. Drag characteristics of v-groove and transverse curvature riblets. *Progress in Astronautics and Aeronautics*, 72:168–184, August 1980.

[16] Tie Wei, Rodney Schmidt, and Patrick Mcmurtry. Comment on the clauser chart method for determining the friction velocity. *Experiments in Fluids*, 38:695–699, 05 2005.